HHS Public Access

Author manuscript

Cell Rep. Author manuscript; available in PMC 2016 January 08.

Published in final edited form as:

Cell Rep. 2015 December 29; 13(12): 2663–2670. doi:10.1016/j.celrep.2015.11.062.

An amacrine cell circuit for signaling steady illumination in the retina

Jason Jacoby[1], **Yongling Zhu**[1], **Steven H. DeVries**[1,2], and **Gregory Schwartz**[1,2]

[1]Department of Ophthalmology, Feinberg School of Medicine, Northwestern University, Chicago, Illinois, 60611

[2]Department of Physiology, Feinberg School of Medicine, Northwestern University, Chicago, Illinois, 60611

Summary

Decades of research have focused on the circuit connectivity between retinal neurons, yet only a handful of amacrine cells have been described functionally and placed in the context of a specific retinal circuit. Here we identify a circuit where inhibition from a specific amacrine cell plays a vital role in shaping the feature selectivity of a postsynaptic ganglion cell. We record from transgenically labeled CRH-1 amacrine cells and identify a postsynaptic target for CRH-1 amacrine cell inhibition in an atypical retinal ganglion cell (RGC) in mouse retina, the Suppressed-by-Contrast (SbC) RGC. Unlike other RGC types, SbC RGCs spike tonically in steady illumination and are suppressed by both increases and decreases in illumination. Inhibition from GABAergic CRH-1 amacrine cells shapes this unique contrast response profile to positive contrast. We show the existence and impact of this circuit with both paired recordings and cell-type specific ablation.

Introduction

The brain contains a multitude of inhibitory interneuron types with diverse computational roles (DeFelipe et al., 2013). Amacrine cells are the most abundant and diverse inhibitory interneuron in the retina, comprising more than 30 morphologically distinct types (Masland, 2012), yet remain the least understood retinal cell class. Only a handful of amacrine cell subtypes have been described functionally and placed in the context of specific retinal circuits (Chen and Li, 2012; Grimes et al., 2010; Lee et al., 2014; Münch et al., 2009; Vaney et al., 2012). The power of genetic manipulations and an advanced knowledge of cell typology are making the mouse retina an increasingly important model system in vision research (Huberman and Niell, 2011). We have taken advantage of these tools to reliably

Corresponding Author: Dr. Gregory Schwartz, greg.schwartz@northwestern.edu.

Author Contributions

J.J. and G.W.S. performed all experiments and data analysis. Y.Z. and S.H.D. provided the original CRH-cre x Ai9 transgenic mice. J.J., G.W.S, and S.H.D. participated in the design of experiments and wrote the manuscript.

target a specific amacrine cell type and place it in a functional microcircuit with a recently identified RGC.

Retinal ganglion cells (RGCs) are typically divided into three categories based on whether they respond with increased firing to light increments (ON cells), decrements (OFF cells), or both (ON-OFF cells). One RGC type, called the Suppressed-by-Contrast (SbC) RGC, does not fit into any of these categories, instead responding by decreasing its firing rate for both increases and decreases in illumination. Since their discovery nearly 50 years ago (Levick, 1967), SbC RGCs have been recorded in cat (Mastronarde, 1985; Troy et al., 1989), rabbit (Sivyer et al., 2010; 2011), and macaque (de Monasterio, 1978), and recently the mouse retina (Tien et al., 2015). Cells with comparable response profiles have been found in downstream visual areas, including the lateral geniculate nucleus (LGN) of the macaque (Tailby et al., 2007), and both the LGN (Piscopo et al., 2013) and primary visual cortex (Niell and Stryker, 2008) of the mouse. SbC cells may play a role in contrast gain modulation, accommodation, and saccadic suppression (Rodieck, 1967; Troy et al., 1989; Tien et al., 2015). While the inhibitory currents that are associated with response suppression have recently been measured in SbC cells (Tien et al., 2015), the circuits responsible for this inhibition have not been identified. Here, we (1) report physiological characterization of CRH-1 amacrine cells, (2) provide direct evidence for connectivity to a postsynaptic RGC, (3) identify the functional role of this retinal microcircuit, and (4) demonstrate a functional change in the SbC RGC following selective ablation of CRH-1 amacrine cells.

Results

Identification and characterization of the Suppressed-by-Contrast RGC

We identified SbC RGCs in a whole-mount *ex vivo* preparation of mouse retina by their responses to a step of light (Figure 1A, black trace, see Experimental Procedures). The SbC RGC's dendrites are bistratified, laminating in the inner plexiform layer (IPL) distal to the OFF choline acetyl transferase (ChAT) band and proximal to the ON ChAT band (Figure 1B). From a mean background illumination of 1000 isomerizations per rod per second (R*/rod/s), we presented spots at a range of positive and negative Weber contrast values. Here and elsewhere, visual stimuli in the form of light or dark spots were projected on to the central portion of the receptive field (see Methods). SbC RGCs exhibited a maintained firing rate in steady illumination (16.2 ± 1.8 Hz, mean ± s.e.m. here and throughout; n = 14), followed by an initial, transient burst of spikes in response to positive contrasts and a period of suppression to both positive and negative contrasts (Figure 1C). Both the number of suppressed spikes (Figure 1E) and the time of suppression (Figure S1A) displayed a characteristic, inverted contrast response function with stronger suppression for higher positive and negative contrasts.

To explore the mechanism responsible for contrast suppression in the SbC RGC, we measured excitatory and inhibitory currents in whole-cell voltage clamp recordings with the same visual stimuli used in the spike recordings Figures 1D and 1F). For negative contrasts, excitation decreased (peak current = 18.6 ± 8.32 pA; n = 4) and inhibition increased (61.4 ± 11.8 pA; Figure 1D, left). For positive contrasts, both excitation and inhibition increased

(exc. = −88.2 ± 19.0 pA; inh. = 369 ± 77.0 pA; n = 4; Figure 1D, right). These synaptic currents explain both the SbC RGC's transient burst at positive contrast (Figures S1C and S1D) and its spike suppression with increased positive and negative contrasts (Figure 1E). Suppression at negative contrasts is controlled by a coordinated decrease in excitation and increase in inhibition; suppression at positive contrasts is controlled by large, sustained inhibition, which overwhelms excitation after its initial transient response (Figure S1). Longer spike suppression times for higher positive contrasts were well matched by a similar trend in the inhibitory currents (Figure S1B). Experiments with receptor antagonists indicated that the inhibitory drive was carried by a combination of $GABA_A$ (53.3 ± 5.4%, *n* = 4) and glycine receptors (46.7 ± 5.4%, *n* = 4)(Figure S2). It is notable that the outer stratum of the SbC RGC's dendritic field is likely exclusively for inhibitory input as we measured no OFF excitation (Figure 1D).

Much like a typical ON RGC, a decrease in excitatory current in the SbC RGC contributes to spike suppression at negative contrasts. For positive contrasts, an increase in excitatory current must be counteracted by inhibition to suppress spiking. Therefore, inhibition is critical to spike suppression of the SbC RGC at positive contrasts. Spike suppression to negative contrast is likely influenced instead by an OFF amacrine cell, but here we focus on the suppression to positive contrast. We sought amacrine cells with two key characteristics as possible sources of this inhibitory drive at positive contrasts. A potential presynaptic amacrine cell would (1) co-stratify with the dendrites of the SbC RGC and (2) depolarize to increases in illumination with a similar sustained time course and dependence on contrast as the SbC RGC's inhibitory current.

Characterization the CRH-1 amacrine cell

We found an amacrine cell matching this morphological and physiological profile in a CRH-cre (corticotrophin releasing hormone) transgenic mouse line. In this line, cre recombinase is expressed in a previously unidentified medium-field GABAergic amacrine cell type, CRH-1 (Zhu et al., 2014). The processes of CRH-1 cells stratified in sublamina 5 of the IPL (Zhu et al., 2014), the same layer as ON dendrites of the SbC RGC. The CRH-1 amacrine cell showed no tracer coupling to nearby amacrine or ganglion cells (Figure 2A). Somata of CRH-1 amacrine cells were displaced and located in the ganglion cell layer, which allowed ease of access for physiological recording. We targeted CRH-1 amacrine cells for whole-cell recordings by two-photon illumination in a cross between a floxed-tdTomato line and the CRH-cre line. CRH-1 amacrine cells responded to a spot of light from darkness with a sustained depolarization of 23.9 ± 1.9 mV (n = 6; Figure 2B). This depolarization was generated by an increase in excitatory current (−219 ± 15.5 pA; n = 9; Figure 2B). Inhibitory currents in CRH-1 amacrine cells were small or absent (Figure S3). The resting membrane potential in the dark was −53.5 ± 1.8 mV (n = 6), and −44.5 ± 2.0 mV (n = 6) at a mean luminance of 1000 R*/rod/s. Peak depolarization increased for positive contrasts in a saturating curve, similar to that observed for the inhibitory currents in the SbC RGC (Figures 1D and 2D). The depolarization of CRH-1 amacrine cells was more prolonged for higher positive contrasts, matching the trend in the inhibitory currents in the SbC RGC (Figures 2C and S1B). CRH-1 amacrine cells label with an antibody to GAD and are

presumptively GABAergic (Zhu et al., 2014), and thus are ideally suited to provide some or all of the GABAergic input to SbC cells.

A direct measurement of synaptic connectivity

The similar time course between the inhibitory current measured in the SbC RGC and the voltage change observed in the CRH-1 amacrine cell led us to hypothesize that CRH-1 amacrine cells could play a role in projecting feedforward inhibition onto the SbC RGC, contributing to spike suppression at positive contrasts. To test whether direct, inhibitory synaptic transmission takes place between the CRH-1 amacrine cell and the SbC RGC, we performed paired recordings between the two cells (Figure 3). We voltage clamped a CRH-1 amacrine cell at −70 mV and began by injecting a 100 mV pulse (50 ms) to maximize GABA release while monitoring inhibitory currents in a nearby SbC RGC held at the reversal potential for excitation. The voltage pulse applied to the presynaptic CRH-1 amacrine cell resulted in a fast outward current in the postsynaptic SbC RGC of 49.9 ± 11.6 pA (n = 5, Figure 3B). This postsynaptic current presumably represents the maximal response from a single presynaptic CRH-1 amacrine cell. The latency from voltage pulse onset to the initiation of the inhibitory current in the postsynaptic cell was 2.9 ± 0.5 ms (latency to peak = 7.7 ± 0.6 ms, n = 5) (Figure 3B, inset), consistent with the timescale of monosynaptic transmission.

We also applied voltage steps that were closer in amplitude to the maximal light response measured in CRH-1 cells by holding at −60 mV and stepping to either −35 or −25 mV. Direct synaptic connectivity was reaffirmed. A 25 mV step produced an 11.24 ± 1.9 pA (n = 3, Figure 3C, top) response in a postsynaptic SbC while a 35 mV depolarization produced a 15.3 ± 1.2 pA current (n = 2, Figure 3C, bottom). Fluorescent imaging confirmed costratification of the dendrites of the CRH-1 amacrine cell and the SbC RGC (Figure 3A). A total of 8 synaptically connected pairs are presented. The distance between the somata of the two recorded cells was < 50 μm for all recorded pairs. We observed no synaptic connectivity in paired recordings between CRH-1 amacrine cells and other costratifying RGC types, including the ON alpha RGC (n = 6, data not shown).

Changes in the SbC computation following ablation of CRH-positive amacrine cells

Our results suggest a direct synaptic input from CRH-1 amacrine cells to SbC RGCs, therefore we set out to determine how removing CRH-1 from the circuit would affect SbC spike output. First, we found a SbC RGC and measured its contrast response function in control conditions. Then tdTomato-positive amacrine cells were identified by multi-photon laser excitation, and cells within a 200 μm radius of the SbC RGC were targeted for physical ablation (Figures 4A and 4B; see Methods). Following the ablation of 25–35 neighboring tdTomato-positive cells, spike suppression to positive contrasts was eliminated; positive contrast stimuli now elicited spiking above the baseline level (Figure 4C). Ablation resulted in the number of spikes from baseline being increased by 146 ± 17% (n = 4, paired t-test $p < .0035$, Figure 4D). The addition of strychnine following ablation, to eliminate glycinergic ON inhibition (Figure S2), further increased the number of spikes above baseline by 274 ± 55% (n = 5, paired t-test $p < .0076$, Figure 4D) to positive contrast. With CRH-1 amacrine cells ablated and glycinergic inhibition blocked, the SbC RGC response profile to light

increments now resembled that of a typical ON RGC. In comparison, the spikes from baseline in recorded control RGCs during the same ablations were altered by just −18 ± 3.7% (n = 5, Figures 4E, 4F, and S4B) in post-ablation conditions. The change between the positive contrast spike count distributions in SbC and control RGCs following ablation was highly significant (Kolmogorov-Smirnov test, $p < .0069$). While the contrast response function of SbC RGCs changed qualitatively following ablation of CRH-1 amacrine cells (from suppression to firing above baseline), all control RGCs (including both ON and OFF types) retained their response polarity following ablation (n = 6, Figure S4B).

Discussion

More than sixty years of research have revealed the morphological diversity of retinal amacrine cells and both the morphological and functional diversity of RGCs, but few synaptic circuits connecting members of these two cell classes have been established. Here we report the a physiological characterization of the CRH-1 amacrine cell, confirm a direct postsynaptic target in the SbC RGC, and establish that the CRH-1 inhibitory input is critical to the SbC computation that mediates suppression to positive contrast. By physically removing CRH-1 from contributing to circuit function, we demonstrate that the SbC RGC no longer displays its characteristic contrast suppression profile to positive contrast (Figure 4).

Our results reveal that CRH-1 amacrine cells release GABA onto the SbC RGC in response to light increments, but our results do not exclude other amacrine cell inputs (Figure 5). Pharmacology results suggest the AII amacrine cell may contribute to glycinergic inhibition to light increments (Figure S2B), but we do not exclude other glycinergic inputs. Other (OFF) amacrine cells are likely responsible for inhibition to light decrements (Figures 1D and 1F).

While we expected the ablation of GABAergic CRH-1 amacrine cells to significantly impact the response of the SbC to positive contrast, a monosynaptic circuit cannot explain the changes observed to negative contrast stimuli after ablation (Figure 4C). CRH-1 ablation reduced the tonic firing rate of the SbC RGC (22.5 Hz in control, 5.5 Hz after ablation, $p = 0.001$, n = 4), thus leaving a smaller dynamic range for suppression to negative contrast. This result suggests a secondary role of CRH-1 in modulating the tonic firing rate of the SbC RGC. A circuit configuration consistent with this result is one in which an unknown amacrine cell tonically inhibits the SbC RGC to set its firing rate in steady illumination. This unknown amacrine in turn is inhibited by the CRH-1 amacrine cell. Thus, ablation of CRH-1 amacrine cells disinhibits the unknown amacrine cell leading to a net increase in inhibition onto the SbC RGC and a decrease in tonic firing. One possible advantage of this proposed serial inhibitory circuit in is that the same amacrine cell (CRH-1) inhibits the SbC RGC through both a sign preserving direct pathway and a sign-inverting indirect pathway so that small noise fluctuations in CRH-1 will tend to cancel, maintaining the fidelity of larger light-induced signals (Cafaro and Rieke, 2010).

The functional roles of amacrine cells are often described as modulatory. Amacrine cell inhibition contributes to the receptive field surround (Farrow et al., 2013), mediates gain

control (Grimes et al., 2009), and alters the kinetics of bipolar cell output (Sagdullaev et al., 2011). We have demonstrated that this amacrine cell circuit instead plays a prominent role in determining the feature selectivity of a postsynaptic retinal ganglion cell. Like the starburst amacrine cell, which is critical to the ON-OFF direction selective circuit (Wei and Feller, 2011), the CRH-1 amacrine cell shapes the unique response profile of the SbC RGC. Perhaps, like CRH-1 cells, other amacrine cell types play specific roles in shaping the feature selectivity of RGCs.

Experimental Procedures

Recording

Wild-type and transgenic mice (CRH-ires-Cre (B6(Cg)-Crh$^{tm1(cre)Zjh}$/J, JAX 012704) were dark adapted overnight. Dissection was performed under IR (900 nm) with assistance from IR visible light converter (night vision) goggles and separate IR dissection scope attachments (BE Meyers, Redmond, WA). Research animals were sacrificed in accordance with all animal care standards provided by Northwestern University. A piece of retina was mounted on a 12 mm poly-D-lysine-coated glass coverslip (BioCoat Cellware, Corning), placed on the electrophysiology rig (SliceScope Pro 6000, Scientifica, UK), superfused with carbogenated Ames medium (Sigma, A-1420; 9 mL/min) warmed to 32°C, and illuminated at 950 nm for visualization. Transgenically labeled amacrine cells (Ai9 x CRH-cre) with displaced somas in the ganglion cell layer were targeted for electrophysiological recording under 2-photon illumination (980 nm, MaiTai HP, SpectraPhysics). The identity of retinal ganglion cells was confirmed with cell-attached capacitive spike responses to light stimuli. Electrophysiological recordings were obtained with a 2-channel patch-clamp amplifier (MultiClamp 700B, Axon Instruments). For voltage clamp experiments, the holding voltage was adjusted for each cell to isolate excitatory and inhibitory currents, starting at −69 and +11 mV, respectively. Voltage clamp recordings used an intracellular solution containing (in mM) the following: 105 Cs methanesulfonate, 10 TEA-Cl, 20 HEPES, 10 EGTA, 2 QX-314, 5 Mg-ATP, and 0.5 Tris-GTP (~270 mOsm; pH ~7.3 with CsOH). Perforated patch recordings of presynaptic CRH-1 amacrine cells in synaptically-coupled paired recordings (Figure 3C only) utilized electrodes that were front-filled with regular cesium-based intracellular solution (see above) and back-filled the same solution with 250 μM β-escin (Sigma-Aldrich). All perforated patch clamp experiments were performed in the presence of the glutamate receptor blockers L-AP4 (20 μM; Tocris) and CNQX (50 μM; Tocris) in order to reduce noise originating from upstream pathways. Due to possible space clamp error in voltage clamping of medium-field CRH-1 amacrine cells (diameter 224 ± 36 μm; (Zhu et al., 2014) through a perforated patch (~40 mOhm access resistance), the 25 mV command voltage is likely an underestimate of the voltage change we achieved at the GABA release sites. When we applied a voltage pulse of 35 mV to the presynaptic CRH-1, we observed an increase in the outward current in the postsynaptic SbC RGC was observed. Current clamp recordings used an intracellular solution containing (in mM) the following: 123 K-aspartate, 10 KCl, 10 HEPES, 1 $MgCl_2$, 1 $CaCl_2$, 2 EGTA, 4 Mg-ATP, and 0.5 Tris-GTP (~270 mOsm; pH ~7.2 with KOH). Absolute voltage values were corrected for a −8.58 mV liquid junction potential in the Cs-based intracellular solution. Pharmacological agents (gabazine, strychnine, and kynurenic acid) were purchased from Sigma.

Visual stimuli

Visual stimuli were presented with a custom-designed light projection device (DLP LightCrafter, Texas Instruments) capable of controlling patterned visual stimulation at frame rates up to 1.4 kHz. All stimuli were focused onto the photoreceptor layer using the microscope's condenser. The device used blue light (450 nm), and light levels are given in the text in R*/rod/s. M cones and S cones were stimulated at rates of 0.45 and 0.02 isomerizations, respectively, per rod isomerization. Light stimuli were centered on the receptive field of each recorded cell. We first measured the cell's response to horizontal and vertical bars across different locations and then adjusted the position of subsequent stimuli to the position that maximized the response in each dimension. Spots of light were 200 μm in diameter, matching the size of the receptive field center for both CRH-1 amacrine cells and SbC RGCs (data not shown). Light steps from darkness were 200 R*/rod/s.

Analysis

Data were analyzed with a custom open-source Matlab analysis package (github.com/SchwartzNU/SymphonyAnalysis), and figures were assembled in Igor 6.3 (Wavemetrics, Portland, OR). The duration and amplitude of the spike suppression response in the SbC RGC (Figures 1D and S1) was calculated as follows. The peri-stimulus time histogram (PSTH) was computed in 10 ms bins and smoothed with a sliding window of 200 ms. The suppression time was measured as the time following stimulus onset at which the smoothed PSTH remained below 50% of the baseline firing rate (measured before stimulus onset). The number of suppressed spikes was measured by subtracting the spikes in the suppression window from the number of spikes expected in this window based on the baseline firing rate. Figure 1E plots the average number of suppressed spikes normalized to the maximum for each cell. Response durations for current and voltage traces (Figure S1B) were measured as the interval over which the average trace exceeded 25% of its maximum value. Onset response times in paired recordings (Figure 3) were based on the time axis intercept of a linear fit to the initial response slope.

Statistics

All data in the paper is reported as mean ± s.e.m. with n-values. We make comparisons for statistical significance with paired t-tests or the Kolmogorov-Smirnov test.

Imaging

For dendritic stratification and morphological imaging, target cells were injected through patch pipettes with Neurobiotin tracer (Vector Laboratories, Burlingame, CA, SP-1150, ~3% w/v and ~280 mOsm in potassium aspartate internal solution). Free-floating whole retinas were blocked in 3% normal donkey serum and incubated in primary antisera against ChAT (Millipore, Temecula, CA, AB144P, goat anti-ChAT, 1:500) with 0.1% sodium azide for 5 nights at 4°C. Following primary incubation and rinses, ChAT-labeled full mount retinas were incubated in secondary antisera against goat IgG (Jackson ImmunoResearch, West Grove, PA, 705-475-147, donkey anti-goat, 1:500) and Streptavidin (Pierce Biotechnology, Rockford, IL, 21832, 1:500), overnight at 4°C. Labeled retinas were mounted on slides and coverslipped with p-phenylenediamine mounting medium.

Synaptically-coupled cells were loaded with AlexaFluor dyes at 488 or 568 nm wavelengths (Life Technologies, A10436, A10437) stimulated using multiphoton excitation at 760 nm. Emission was split into two channels with a dichroic mirror and collected by bandpass emission filters (520–540 nm for AlexaFluor 488; 580–640 nm for AlexaFluor 568).

All fixed tissues were imaged on a Nikon A1R laser scanning confocal microscope mounted on a Nikon Ti ZDrive PerfectFocus microscope stand equipped with an inverted 60x oil immersion objective (Nikon Plan Apo VC 60x/1.4 NA). Streptavadin and AlexaFluor 488 fluorescence was stimulated at 488 nm (emission collected at 530 nm and above) and ChAT labeling was stimulated at 405 nm (emission collected at 450 nm and above). All confocal images were collected in 0.2 μM steps in the z-axis. Confocal imaging was performed at the Nikon Imaging Center at Northwestern University's Feinberg School of Medicine using Nikon Elements software. Images were analyzed using ImageJ / Fiji.

Ablation

The contrast response function of an identified SbC RGC and a nearby control RGC were obtained with a cell attached recording. The pipettes were removed and then tdTomato-positive amacrine cells within a 200 μm radius of the SbC RGC were identified by 2-photon excitation (980 nm) and targeted for physical ablation. Using multi-photon laser guidance, the tip of a sharp electrode backfilled with Ames solution and AlexaFluor 488 was used to pierce the inner limiting membrane and penetrate the cell membrane of the targeted tdTomato-positive amacrine cell. Electrical access into the cell was confirmed by its negative resting potential and a rapid cell fill of AlexaFluor 488 and subsequent colocalization with the tdTomato reporter. A 20 nA square pulse at a frequency of 10 kHz was then injected into the cell for 5–10 seconds until the destruction of the cell was confirmed visually by the rupture of the cell membrane. Cell death was also confirmed with the absence of the AlexaFluor 488 fill and tdTomato reporter under 2-photon illumination. Approximately 25–35 tdTomato-positive cells were present within the 200 μm radius of the SbC RGC; these cells were ablated prior to revisiting the SbC RGC and control RGC and recording their light responses in the cell attached mode. The membrane of the SbC RGC under the pipette was then ruptured and tracer was allowed to diffuse into the cell. An image stack was acquired before and after CRH ablation in the 300 μm × 300 μm area surrounding the SbC RGC.

Supplementary Material

Refer to Web version on PubMed Central for supplementary material.

Acknowledgments

We thank our lab manager, Susan Wohlgenant, for her extensive experimental preparation and technical assistance. We also thank William Grimes, Michael Manookin, Fred Rieke, and Haohua Qian for their commentary on early drafts of the manuscript. Thank you to William Grimes for his advice on the ablation technique and Sercan Deniz for his guidance on perforated patch.

Funding

This research project was funded by the Ruth L. Kirschstein National Research Service Award (NRSA) Postdoctoral Fellowship 1F32EY025930-01, NIH DP2-DEY026770A, and the Research to Prevent Blindness Career Development Award.

References

Cafaro J, Rieke F. Noise correlations improve response fidelity and stimulus encoding. Nature. 2010; 468:964–967. [PubMed: 21131948]

Chen S, Li W. A color-coding amacrine cell may provide a blue-off signal in a mammalian retina. Nat Neurosci. 2012; 15:954–956. [PubMed: 22634731]

de Monasterio FM. Properties of ganglion cells with atypical receptive-field organization in retina of macaques. Journal of Neurophysiology. 1978; 41:1435–1449. [PubMed: 104014]

DeFelipe J, López-Cruz PL, Benavides-Piccione R, Bielza C, Larrañaga P, Anderson S, Burkhalter A, Cauli B, Fairén A, Feldmeyer D, et al. New insights into the classification and nomenclature of cortical GABAergic interneurons. Nat Rev Neurosci. 2013; 14:202–216. [PubMed: 23385869]

Farrow K, Teixeira M, Szikra T, Viney TJ, Balint K, Yonehara K, Roska B. Ambient Illumination Toggles a Neuronal Circuit Switch in the Retina and Visual Perception at Cone Threshold. Neuron. 2013; 78:325–338. [PubMed: 23541902]

Grimes WN, Li W, Chávez AE, Diamond JS. BK channels modulate pre- and postsynaptic signaling at reciprocal synapses in retina. Nat Neurosci. 2009; 12:585–592. [PubMed: 19363492]

Grimes WN, Schwartz GW, Rieke F. The Synaptic and Circuit Mechanisms Underlying a Change in Spatial Encoding in the Retina. Neuron. 2014; 82:460–473. [PubMed: 24742466]

Grimes WN, Zhang J, Graydon CW, Kachar B, Diamond JS. Retinal Parallel Processors: More than 100 Independent Microcircuits Operate within a Single Interneuron. Neuron. 2010; 65:873–885. [PubMed: 20346762]

Huberman AD, Niell CM. What can mice tell us about how vision works? Trends in Neurosciences. 2011; 34:464–473. [PubMed: 21840069]

Ke JB, Wang YV, Borghuis BG, Cembrowski MS, Riecke H, Kath WL, Demb JB, Singer JH. Adaptation to Background Light Enables Contrast Coding at Rod Bipolar Cell Synapses. Neuron. 2014; 81:388–401. [PubMed: 24373883]

Lee S, Chen L, Chen M, Ye M, Seal RP, Zhou ZJ. An Unconventional Glutamatergic Circuit in the Retina Formed by vGluT3 Amacrine Cells. Neuron. 2014; 84:708–715. [PubMed: 25456497]

Levick WR. Receptive fields and trigger features of ganglion cells in the visual streak of the rabbits retina. The Journal of Physiology. 1967; 188:285–307. [PubMed: 6032202]

Manookin MB, Beaudoin DL, Ernst ZR, Flagel LJ, Demb JB. Disinhibition Combines with Excitation to Extend the Operating Range of the OFF Visual Pathway in Daylight. Journal of Neuroscience. 2008; 28:4136–4150. [PubMed: 18417693]

Masland RH. The Neuronal Organization of the Retina. Neuron. 2012; 76:266–280. [PubMed: 23083731]

Mastronarde DN. Two types of cat retinal ganglion cells that are suppressed by contrast. Vision Research. 1985; 25:1195–1196. [PubMed: 4071998]

Murphy GJ, Rieke F. Signals and noise in an inhibitory interneuron diverge to control activity in nearby retinal ganglion cells. Nat Neurosci. 2008; 11:318–326. [PubMed: 18223648]

Münch TA, da Silveira RA, Siegert S, Viney TJ, Awatramani GB, Roska B. Approach sensitivity in the retina processed by a multifunctional neural circuit. Nat Neurosci. 2009; 12:1308–1316. [PubMed: 19734895]

Niell CM, Stryker MP. Highly selective receptive fields in mouse visual cortex. J Neurosci. 2008; 28:7520–7536. [PubMed: 18650330]

Piscopo DM, El-Danaf RN, Huberman AD, Niell CM. Diverse Visual Features Encoded in Mouse Lateral Geniculate Nucleus. Journal of Neuroscience. 2013; 33:4642–4656. [PubMed: 23486939]

Rodieck RW. Receptive fields in the cat retina: a new type. Science. 1967; 157:90–92. [PubMed: 6026674]

Sagdullaev BT, Eggers ED, Purgert R, Lukasiewicz PD. Nonlinear interactions between excitatory and inhibitory retinal synapses control visual output. J Neurosci. 2011; 31:15102–15112. [PubMed: 22016544]

Sivyer B, Taylor WR, Vaney DI. Uniformity detector retinal ganglion cells fire complex spikes and receive only light-evoked inhibition. Proc Natl Acad Sci USa. 2010; 107:5628–5633. [PubMed: 20212117]

Sivyer B, Venkataramani S, Taylor WR, Vaney DI. A novel type of complex ganglion cell in rabbit retina. J Comp Neurol. 2011; 519:3128–3138. [PubMed: 21800303]

Stone TW, Burton NR. NMDA receptors and ligands in the vertebrate CNS. Prog Neurobiol. 1988; 30:333–368. [PubMed: 2830636]

Tailby C, Solomon SG, Peirce JW, Metha AB. Two expressions of "surround suppression" in V1 that arise independent of cortical mechanisms of suppression. Vis Neurosci. 2007; 24:99–109. [PubMed: 17430613]

Tien NW, Pearson JT, Heller CR, Demas J, Kerschensteiner D. Genetically identified suppressed-by-contrast retinal ganglion cells reliably signal self-generated visual stimuli. J Neurosci. 2015; 35(30):10815–10820. [PubMed: 26224863]

Troy JB, Einstein G, Schuurmans RP, Robson JG, Enroth-Cugell C. Responses to sinusoidal gratings of two types of very nonlinear retinal ganglion cells of cat. Vis Neurosci. 1989; 3:213–223. [PubMed: 2487103]

Vaney DI, Sivyer B, Taylor WR. Direction selectivity in the retina: symmetry and asymmetry in structure and function. Nat Rev Neurosci. 2012; 13:194–208. [PubMed: 22314444]

Wei W, Feller MB. Organization and development of direction-selective circuits in the retina. Trends in Neurosciences. 2011; 34:638–645. [PubMed: 21872944]

Zhu Y, Xu J, Hauswirth WW, DeVries SH. Genetically Targeted Binary Labeling of Retinal Neurons. Journal of Neuroscience. 2014; 34:7845–7861. [PubMed: 24899708]

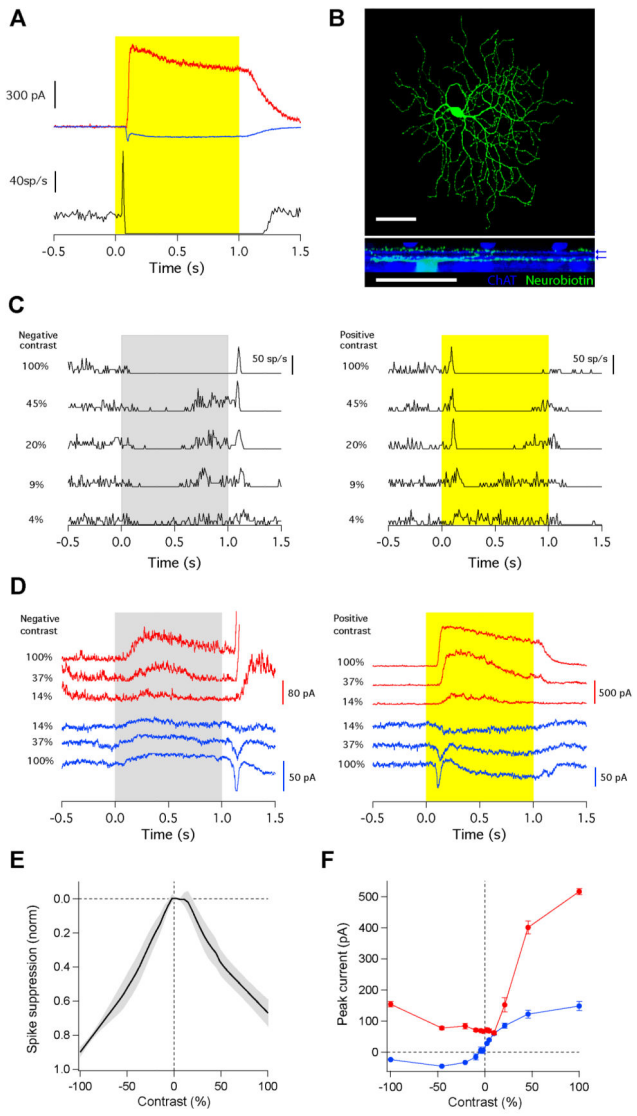

Figure 1.

The Suppressed-by-Contrast retinal ganglion cell. (**A**) Spike responses to a step of light from darkness to 200 R*/rod/s (highlight) measured in cell-attached configuration (black) and in voltage-clamp to isolate excitatory (blue) and inhibitory (red) currents. (**B**) Morphology of the ganglion cell in z-projection. *Bottom*, side view showing stratification profile along with ChAT bands (blue), location marked with blue arrows. Scale bars are 50 μm. (**C**) Spike responses to spots of varying negative (left) and positive (right) contrast presented to the receptive field center from a mean of 1000 R*/rod/s. (**D**) Peak excitatory (blue; excitatory current inverted for comparison) and inhibitory (red) synaptic currents in response to negative (left) and positive (right) contrast steps. (**E**) Normalized spike suppression versus contrast calculated across cells from data as in **C**. Shaded regions are s.e.m, n = 14 cells. (**F**) Average current traces from the cell depicted in **D**. Note the difference in scale between inhibitory currents for positive and negative contrast. Error bars are s.e.m. across trials for a single cell, n = 10 trials.

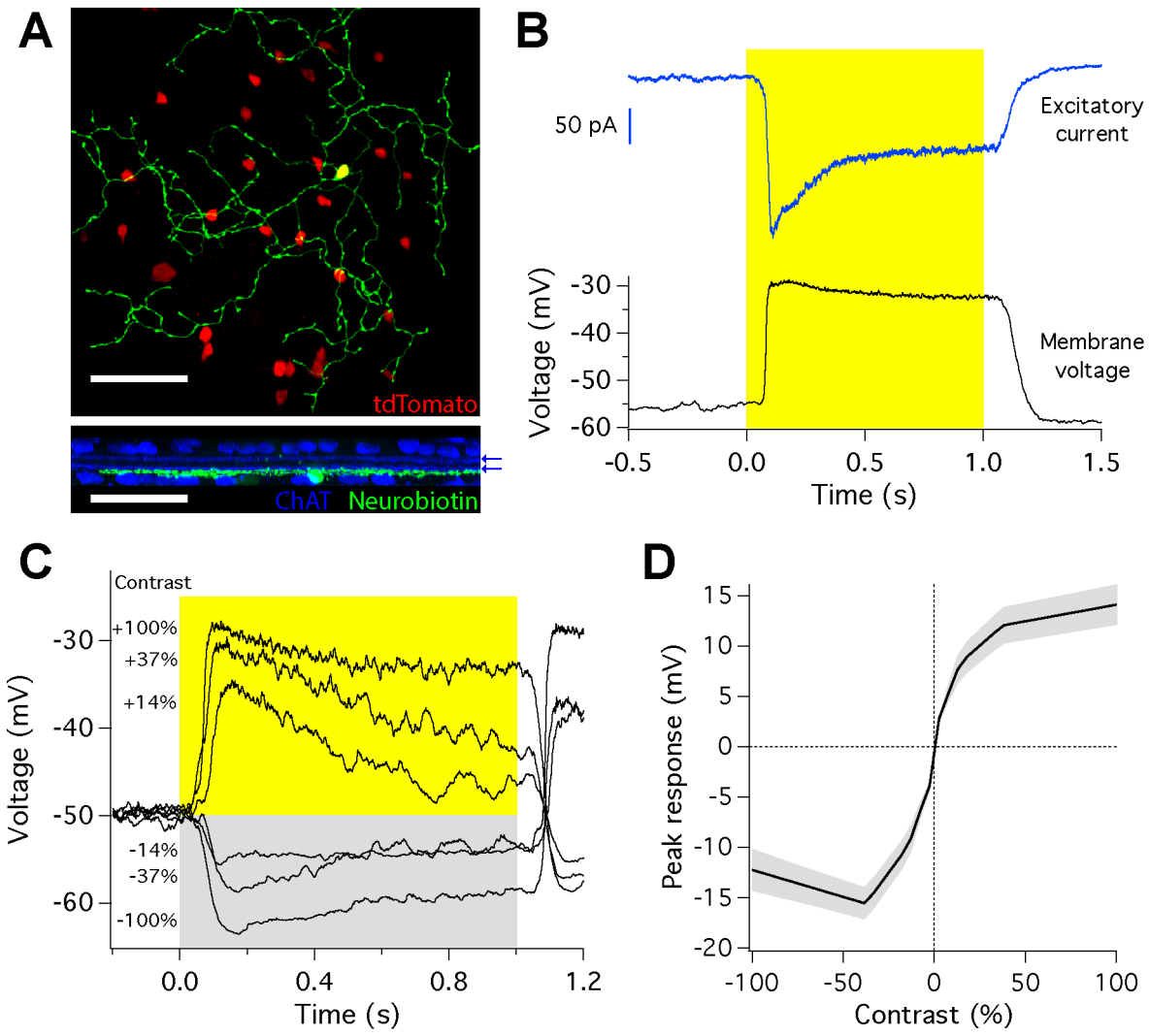

Figure 2.

The CRH-1 amacrine cell. (**A**) Morphology of a CRH-1 amacrine cell filled with neurobiotin (green) in the reporter line expressing tdTomato (red). *Bottom*, side view showing dendritic stratification with ChAT bands (blue), location marked with blue arrows. Scale bar is 50 μm. (**B**) Response of the amacrine cell to a step of light from darkness to 200 R*/rod/s. *Bottom*, membrane potential measured in current clamp. *Top*, excitatory synaptic current measured in voltage clamp. Traces are averages of 10 trials. (**C**) Membrane potential in response to steps across a range of positive and negative contrasts from a mean of 1000 R*/rod/s. Traces are averages of 10 trials. (**D**) Average relationship between peak voltage response and contrast. Shaded region is s.e.m., $n = 6$ cells.

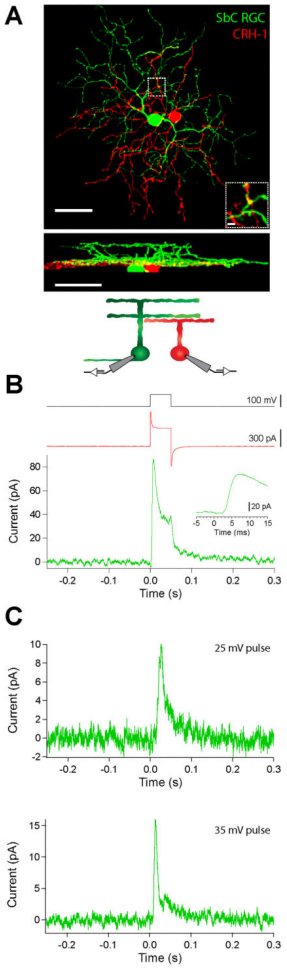

Figure 3.

CRH-1 amacrine cells provide direct inhibition to SbC RGCs. (**A**) Image of nearby SbC RGC (green) and CRH-1 amacrine cell (red) in z-projection (*top*), side view (*middle*), and circuit schematic (*bottom*). Scale bar is 50 μm. Inset displays magnification of the boxed region showing site of possible interaction between CRH-1 amacrine cell and SbC RGC dendrites in a 2 μm plane of the image stack. Scale bar is 5 μm. (**B**) Representative inhibitory current in the SbC RGC (green) measured while injecting a voltage pulse into a nearby CRH-1 amacrine cell with whole cell patch access (red). Capacitive transients in CRH-1 amacrine cell current truncated for clarity. *Inset*, magnification of the response onset to peak. (**C**) Representative inhibitory current in the SbC RGC (green) measured while injecting a 25 mV (*top*) and 35 mV (*bottom*) voltage pulse into a nearby CRH-1 amacrine cell with perforated patch access and in the presence of glutamate receptor antagonists (see Methods). Traces are averages of 100 trials for traces in **B** and **C**.

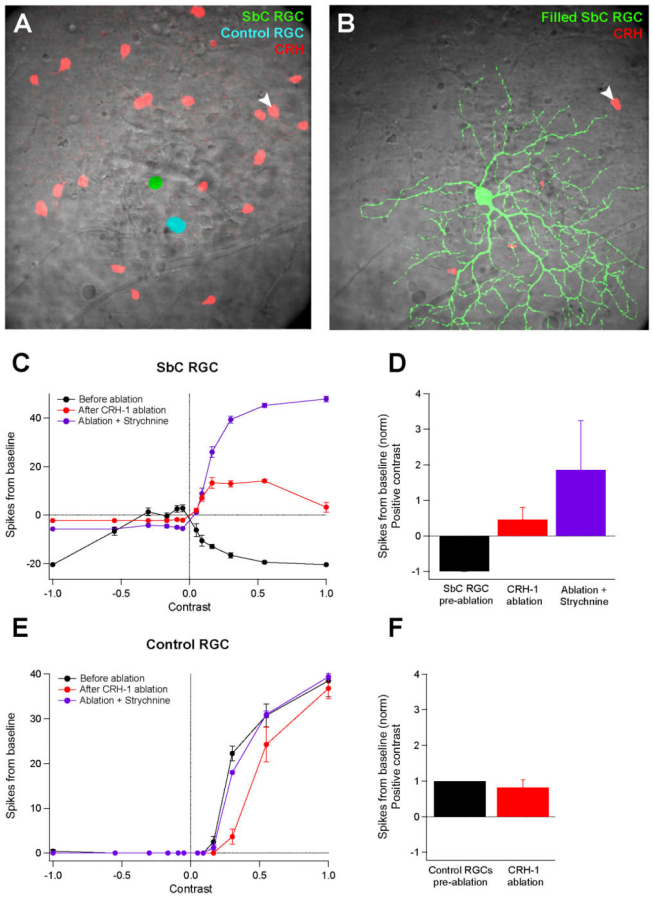

Figure 4.

Ablation of CRH-1 amacrine cells dramatically alters the response profile of SbC RGCs to positive contrast. (**A**) DIC image of the pre-ablation retina overlayed with fluorescence of tdTomato labeled amacrine cells (red). Location of the recorded SbC RGC is pseudocolored in green and the control ON RGC in cyan. (**B**) DIC image of the post-ablation retina containing the SbC RGC filled with AlexaFluor 488 (green) and a spared tdTomato-positive amacrine cell (red, marked with white arrowhead). Scale bars are 50 μm. Cell-attached recordings from the SbC RGC (**C**) and control RGC (**E**) displaying the total number of spikes from baseline to positive and negative contrast. Traces are averages of 5–9 trials and error bars are s.e.m. Population data to positive contrast for SbC RGCs (**D;** n = 5, 4, 5 in pre-ablation, post-ablation, and ablation + strychnine, respectively) and control RGCs (**F;** n = 6 for both conditions) in the pre-ablation environment (black), post-ablation environment (red), or post-ablation in the presence of 1 μM strychnine (purple). Error bars are s.e.m. across cells. Each cell recorded was normalized to pre-ablation conditions.

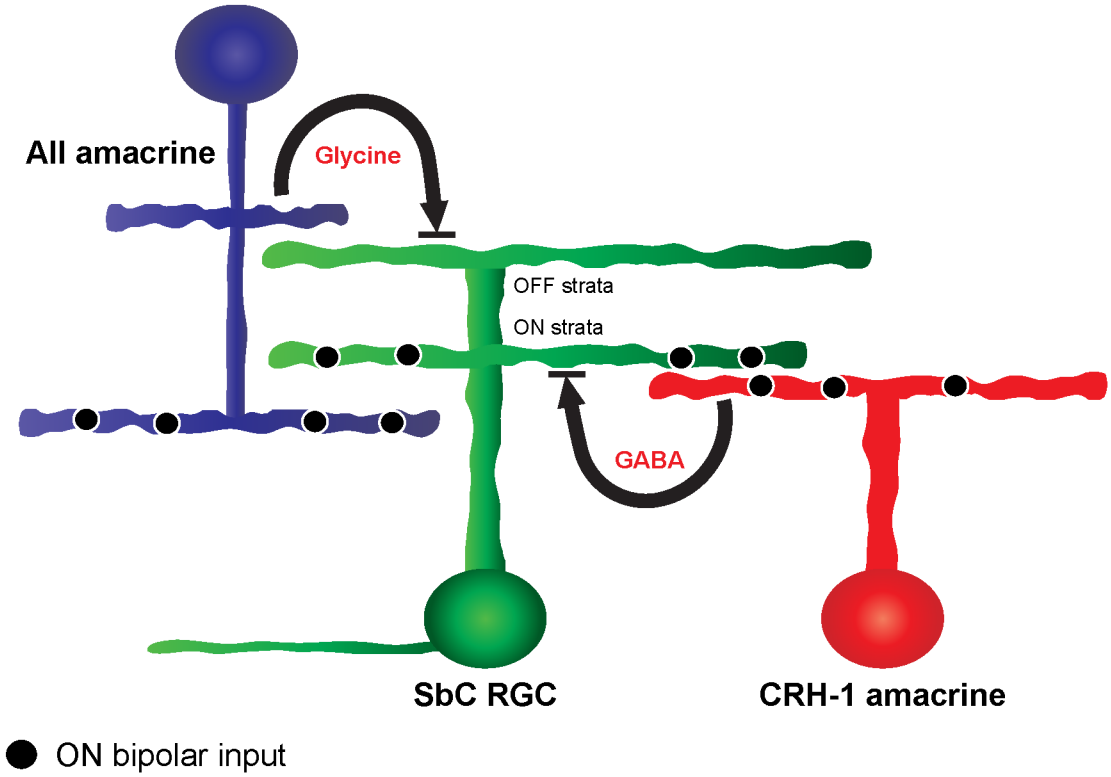

Figure 5.

Schematic of circuitry mediating suppression to positive contrast in the SbC RGC. SbC RGCs receive GABAergic inhibition from CRH-1 amacrine cells and glycinergic inhibition from AII amacrine cells. Both of these inhibitory circuits contribute to spike suppression to positive contrasts, and both are necessary. Note that unknown circuit components (e.g. the identity of bipolar cell inputs and amacrine cell inputs for negative contrast suppression) are not shown (see Discussion).